Mon. Not. R. Astron. Soc. **000**, 000–000 (0000) Printed 17 January 2011 (MN LATEX style file v2.2)

Locating positions of γ-ray–emitting regions in blazars

H. T. Liu[1,2⋆], J. M. Bai[1,2⋆] and J. M. Wang[3,4⋆]
[1] *National Astronomical Observatories/Yunnan Astronomical Observatory, Chinese Academy of Sciences, Kunming, Yunnan 650011, China*
[2] *Key Laboratory for the Structure and Evolution of Celestial Objects, Chinese Academy of Sciences, Kunming, Yunnan 650011, China*
[3] *Key Laboratory for Particle Astrophysics, Institute of High Energy Physics, Chinese Academy of Sciences, 19B Yuquan Road, Beijing 100049, China*
[4] *Theoretical Physics Center for Science Facilities, Chinese Academy of Sciences, Beijing 100049, China*

Accepted . Received

ABSTRACT

We propose a new method to locate the γ-ray–emitting positions R_γ from the measured time lags $\tau_{\rm ob}$ of γ-ray emission relative to broad emission lines. The method is also applicable to lower frequencies. R_γ depends on parameters $\tau_{\rm ob}$, $R_{\rm BLR}$, $v_{\rm d}$ and θ, where $R_{\rm BLR}$ is the size of broad-line region, $v_{\rm d}$ is the travelling speed of disturbances down the jet and θ is the viewing angle of the jet axis to the line of sight. As $\tau_{\rm ob} = 0$, $\tau_{\rm ob} < 0$ or $\tau_{\rm ob} > 0$, the broad lines zero-lag, lag or lead the γ-rays, respectively. It is applied to 3C 273, in which the lines and the radio emission have enough data, but the γ-rays have not. We find $\tau_{\rm ob} < 0$ and $\tau_{\rm ob} > 0$ for the 5, 8, 15, 22 and 37 GHz emission relative to the broad lines Hα, Hβ and Hγ. The lag may be positive or negative, however current data do not allow to discriminate between the two cases. The measured lags are on the order of years. For a given line, $\tau_{\rm ob}$ generally decreases as radio frequency increases. This trend most likely results from the radiative cooling of relativistic electrons. The negative lags have an average of $\tau_{\rm ob} = -2.86$ years for the 37 GHz emission, which represents that the lines lag the radio emission. The positive lags have $\tau_{\rm ob} = 3.20$ years, which represents that the lines lead the radio emission. We obtain the radio emitting positions $R_{\rm radio} = 0.40$–2.62 pc and $R_{\rm radio} = 9.43$–62.31 pc for the negative and positive lags, respectively. From the constraint of $R_\gamma \lesssim R_{\rm radio}$ (e.g. Dermer & Schlickeiser 1994; Jorstad et al. 2001), we have $R_\gamma \lesssim 0.40$–2.62 pc for the negative lags. For the positive lags, 4.67–$30.81 < R_\gamma \lesssim 9.43$–$62.31$ pc. These estimated R_γ are consistent with those of other researches. These agreements confirm the reliability of the method and assumptions. The method may be also applicable to BL Lacertae objects, in which broad lines were detected.

Key words: γ-rays: theory – galaxies: active – galaxies: jets – quasars: emission lines – quasars: individual: 3C 273.

1 INTRODUCTION

The γ-rays of blazars are generally believed to be generated by inverse Compton (IC) emission from a relativistic jet oriented at a small angle to the line of sight (Blandford & Rees 1978). Two of the most accepted scenarios for broad-band emission from radio to γ-rays are the synchrotron self-Compton (SSC) and external Compton (EC) models (see e.g. Ghisellini et al. 1998). The broad-band spectral energy distributions (SEDs) of blazars consist of two broad bumps (see e.g. Fossati et al. 1998; Ghisellini et al. 1998). The first component is from the synchrotron process, and the second one, generally peaking at the γ-ray regime, is generated by the IC emission of the same electron population responsible for the synchrotron emission (see e.g. Ghisellini et al. 1998; Böttcher 1999). However, the positions of γ-ray–emitting regions are still an open and controversial issue in the researches on blazars. It was suggested that γ-rays are produced within broad-line region (BLR) and that the γ-ray–emitting positions R_γ range roughly between 0.03 and 0.3 parsec (pc) (Ghisellini & Madau 1996). Blandford & Levinson (1995) also suggested a sub-pc γ-ray–emitting region. It was argued that the radiative plasma in relativistic jets of powerful blazars are inside the BLR (Georganopoulos, Kirk & Mastichiadis 2001). On the con-

⋆ E-mail: htliu@ynao.ac.cn; baijinming@ynao.ac.cn; wangjm@mail.ihep.ac.cn

trary, it was also argued that the γ-ray–emitting regions are outside the BLR (Lindfors, Valtaoja & Türler 2005; Sokolov & Marscher 2005). Internal absorption for 10 GeV–1 TeV γ-rays were used to constrain R_γ (Liu & Bai 2006; Liu, Bai & Ma 2008; Bai, Liu & Ma 2009). Variability of the high energy flux indicates that the γ-ray–emitting positions cannot be too distant from the central supermassive black hole (Ghisellini & Madau 1996; Ghisellini & Tavecchio 2009), while the photon-photon absorption implies that the emitting positions cannot be too close to the black hole and its accretion disc (Ghisellini & Madau 1996; Wang 2000; Liu & Bai 2006; Liu, Bai & Ma 2008; Sitarek & Bednarek 2008; Bai, Liu & Ma 2009; Ghisellini & Tavecchio 2009; Tavecchio & Mazin 2009). Bracketed by the two limits, one obtains a few hundreds of Schwarzschild radii as the preferred jet location where most of the dissipation occurs (Ghisellini & Tavecchio 2009). Jorstad et al. (2001) established a connection between ejections of superluminal radio knots and γ-ray outbursts observed by EGRET. They concluded that the radio and γ-ray events are originating from the same region of a relativistic jet. Wagner (2008) found that the blazar γ-ray emission might depend on the mass of the central black hole and that very high energy (VHE) γ-ray–emitting active galactic nuclei (AGNs) have the black hole masses larger than 10^8 solar masses. Bloom (2008) confirmed the radio and γ-ray correlation of EGRET blazars. Thompson (2008) reported that a central feature of the EGRET results is the high degree of variability seen in many γ-ray sources, indicative of the powerful central engines at work in objects visible to γ-ray telescopes.

The operation of *Fermi Gamma Ray Space Telescope* (*Fermi*)–Large Area Telescope (LAT) (see e.g. Abdo et al. 2009, 2010a) presents an exceptional opportunity for understanding the central engines operating in blazars. The First LAT AGN Catalog includes 709 AGNs, comprising 300 BL Lacertae objects (BL Lacs), 296 flat spectrum radio quasars (FSRQs), 41 AGNs of other types and 72 AGNs of unknown types (Abdo et al. 2010a). The distribution of γ-ray photon spectral index is found to correlate strongly with blazar subclass (Abdo et al. 2010a,c). Abdo et al. (2010b) found for *Fermi* blazars that variation amplitudes are larger for FSRQs and low/intermediate synchrotron frequency peaked BL Lacs. Ghisellini, Tavecchio & Ghirlanda (2009) obtained a few hundreds of Schwarzschild radii as the preferred jet dissipation region. Ghisellini et al. (2010) found for bright *Fermi* blazars that the jet dissipation region is within the BLR for FSRQs. Kovalev et al. (2009) identified the pc-scale radio core as a likely location for both the γ-ray and radio flares. Sikora et al. (2009) suggested that the blazar emission zone is located at pc-scale distances from the nucleus, and they also proposed that the pc-scale blazar activity can be occasionally accompanied by dissipative events taking place at sub-pc distances. Ghisellini, Maraschi & Tavecchio (2009) argued that the bulk of the most luminous blazars already detected by *Fermi* should be characterized by large black hole masses, around 10^9 solar masses. Kovalev et al. (2009) found for *Fermi* blazars that the γ-ray photon flux correlates with the compact radio density flux.

Disturbances in the central engine are likely transported down the relativistic jets. This was supported by observations that dips in the X-ray emission are followed by ejections of bright superluminal knots in the radio jets of AGNs and microquasars (e.g. Marscher et al. 2002; Chaterjee et al. 2009; Arshakian et al. 2010). The events in the central engine, where the X-rays are produced, will have a direct effect on the events in the radio jets (e.g. Marscher et al. 2002; Chaterjee et al. 2009). The disc-jet connection was suggested by correlations of emission line luminosity and radio power of jets for various samples of AGNs (Rawlings & Saunders 1991; Falcke, Malkan & Biermann 1995; Celotti, Padovani & Ghisellini 1997; Serjeant et al. 1998; Cao & Jiang 1999, 2001; Wang & Ho 2003; Gu, Cao & Jiang 2009). The relativistic jets can be ejected from inner accretion disc in the vicinity of the central black hole (see e.g. Penrose 1969; Blandford & Znajek 1977; Blandford & Payne 1982; Meier, Koide & Uchida 2001). The close connection between accretion disc and jets indicates that the central disturbances are likely transported down the jets. For example, the central disturbances that drive variations of the central ionizing continuum may be transported with the outward Alfvén waves (see e.g. Meier, Koide & Uchida 2001; Koide et al. 2002). By magnetohydrodynamic mechanisms (Kudoh & Shibata 1999), the transported disturbances may be converted into the local energies of plasma far from the central black hole. Thus the disturbances in the central engine would influence the γ-rays emitted by the relativistic jet aligned with the line of sight. At the same time, these disturbances can lead to the variations of the central ionizing continuum that drives broad emission lines from BLR. Hence, the broad lines from the BLR and the γ-rays from the relativistic jet may be both coupled to the disturbances in the central engine.

Based on the photoionization assumption and the time lags between broad lines and continuum, reverberation mapping observations are able to determine the sizes of the BLRs for type 1 AGNs (see e.g. Kaspi & Netzer 1999; Wandel, Peterson & Malkan 1999; Kaspi et al. 2000, 2005, 2007; Peterson et al. 2000, 2004, 2005; Vestergaard & Peterson 2006). According to the reverberation mapping model (e.g. Blandford & McKee 1982), the variations of broad lines can reflect the disturbances in the central engines of blazars, even though the beamed emission from the relativistic jet strongly affects the real ionizing continuum from accretion disc so that no appropriate continuum could be used as the reference to estimate the time lags relative to the broad lines. If the broad lines from the BLR and the γ-rays from the relativistic jet are both coupled to the disturbances in the central engine, the disturbances should similarly influence both variations of the γ-rays and the broad lines. Thus there should be correlations and time lags between the broad lines and the γ-rays. The time lags should be related to R_γ. In the paper, we attempt to locate R_γ from the time lags between both variations of the broad lines from the BLR and the γ-rays from the relativistic jet.

2 METHOD

The broad lines from the BLR and the γ-rays from the relativistic jet may be both coupled to the disturbances in the central engine. Thus the disturbances could similarly influence both variations of the broad lines and the γ-rays emitted by the jet aligned with the line of

sight. The outbursts seen in light curves are physically linked to the ejections of superluminal radio knots (e.g. Türler, Courvoisier & Paltani 2000). The events in the central engine will have a direct effect on the events in the radio jets (e.g. Marscher et al. 2002; Chaterjee et al. 2009). Thus it is likely that the γ-ray outbursts are caused by the disturbances from the central engine, but not the local disturbances produced in the jets. Hence, there should be correlations between the γ-ray outbursts and the variations of broad lines. It is possible that there are time lags in the correlations and the time lags are related to the positions R_γ. Thus R_γ could be located by the time lags between the γ-ray outbursts and the variations of broad lines. In the future, the quasi-simultaneous observations of γ-rays with *Fermi*/LAT and broad lines with optical telescopes on the order of years may be employed to test this expectation. The method of locating R_γ is also applicable to infrared, optical and radio emission.

First, it is assumed that the disturbances in the central engine are transported outward by some process, and the disturbances could similarly influence both variations of the broad lines from the BLR and the γ-rays from the relativistic jet aligned with the line of sight. Second, we assume a simple geometry (see Fig. 1*a*) that is similar to the schemes in the classical reverberation mapping of the broad lines (see e.g. Kaspi & Netzer 1999; Wandel, Peterson & Malkan 1999; Kaspi et al. 2000, 2005, 2007; Peterson et al. 2000, 2004, 2005; Vestergaard & Peterson 2006). The differences between this method and the classical mapping are as follows. In the classical mapping, a part of ionizing continuum drives the broad lines from the BLR, and another directly reaches observers. Thus the broad lines lag the continuum due to light travelling time effects, and the time lag corresponds to the size of the BLR. In the method proposed here, the ionizing photon signals directly detected by telescopes in the classical mapping are replaced with the transporting disturbances from the central engine down the jet and then with the jet emission signals at R_γ. Thus the method would be valid even if the BLR has a complex configuration, such as a spherical shell. For simplicity for graphic illustration, we choose the BLR to be a ring (see Fig. 1*a*). The transporting speed of disturbances down the jet cannot exceed the speed of light.

Because R_γ is unknown, the γ-rays may lag, lead or zero-lag the broad lines. First, we try to find the position where the γ-rays are produced and zero-lag the broad lines. As the disturbances reach point G (see Fig. 1*a*), where the γ-rays are produced, i.e. $R_\gamma = AG$, the ionizing continuum photons travel from point A to B and the line photons travel from point B to I in time interval R_γ/v_d. In the case of zero-lag (hereafter Case A), we have $(R_\mathrm{BLR} + R_\gamma)/c = R_\gamma/v_\mathrm{d}$, and then

$$R_\gamma = R_\mathrm{BLR}\frac{v_\mathrm{d}}{c - v_\mathrm{d}}, \tag{1}$$

where v_d is the travelling speed of disturbances down the jet and c is the speed of light. For Case A, $R_\gamma > R_\mathrm{BLR}$.

Within segment AG, the lines will lag the γ-rays. As the disturbances reach point F, where the γ-rays are produced, i.e. $R_\gamma = AF$, the ionizing continuum photons reach point E. The light travelling time effects for the ionizing photons from point E to B and the line photons from B to K result in the time lag of the lines relative to the γ-rays (see Fig. 1*a*). In this case (hereafter Case B), we have $R_\gamma + R_\mathrm{BLR} - R_\gamma c/v_\mathrm{d} = c\tau_\mathrm{ob}/(1+z)$, and then

$$R_\gamma = \frac{R_\mathrm{BLR} - \frac{c\tau_\mathrm{ob}}{1+z}}{\frac{c}{v_\mathrm{d}} - 1}, \tag{2}$$

where z is the redshift of source, $\tau_\mathrm{ob} > 0$ and τ_ob is the observed time lag of the broad lines relative to the γ-rays.

Outside segment AG, the γ-rays will lag the lines. As the disturbances reach point H, where the γ-rays are produced, i.e. $R_\gamma = AH$, the line photons reach point L. The light travelling time effects for the γ-ray photons from point J to L, i.e. from point H to M, result in the time lag of the γ-rays relative to the lines (see Fig. 1*a*). In this case (hereafter Case C), we have $R_\gamma c/v_\mathrm{d} = R_\gamma + R_\mathrm{BLR} + c\tau_\mathrm{ob}/(1+z)$, and then

$$R_\gamma = \frac{R_\mathrm{BLR} + \frac{c\tau_\mathrm{ob}}{1+z}}{\frac{c}{v_\mathrm{d}} - 1}, \tag{3}$$

where $\tau_\mathrm{ob} > 0$ and τ_ob is the observed time lag of the γ-rays relative to the broad lines. Equations (1), (2) and (3) can be unified into

$$R_\gamma = \frac{R_\mathrm{BLR} + \frac{c\tau_\mathrm{ob}}{1+z}}{\frac{c}{v_\mathrm{d}} - 1}, \tag{4}$$

where τ_ob is the observed time lags of the γ-rays relative to the broad lines and is zero, negative or positive. As $\tau_\mathrm{ob} = 0$ (Case A), equation (4) becomes equation (1). As $\tau_\mathrm{ob} < 0$ (Case B), equation (4) becomes equation (2). As $\tau_\mathrm{ob} > 0$ (Case C), equation (4) becomes equation (3). Once τ_ob, R_BLR and v_d are known, R_γ can be obtained from equations (1)–(4).

The calculations above are under the condition of $\theta = 0$, where θ is the angle between the jet axis and the line of sight. In fact, the approaching relativistic jets of blazars are oriented at a small angle to the line of sight (Blandford & Rees 1978). Thus $\theta \neq 0$. Considering the actual inclination of the jet axis with respect to the line of sight (see Fig. 1*b*), we rededuce the expression of Case C. As the disturbances reach point H, where the γ-rays are produced, the line photons reach point L. The light travelling time effects for the γ-ray photons from point O to L, i.e. from point H to S, result in the time lag of the γ-rays relative to the lines (see Fig. 1*b*). In this case, we have $R_\gamma c/v_\mathrm{d} = R_\mathrm{BLR} + R_\gamma\cos\theta + c\tau_\mathrm{ob}/(1+z)$, and then

$$R_\gamma = \frac{R_\mathrm{BLR} + \frac{c\tau_\mathrm{ob}}{1+z}}{\frac{c}{v_\mathrm{d}} - \cos\theta}. \tag{5}$$

It is obvious that equation (5) contains Cases A, B and C. As $\theta = 0$, equation (5) becomes equation (4). The observed line photons are from the BLR of ring, and then the observed lag is an ensemble average over all points of the ring. For point T, we have $R_\gamma c/v_\mathrm{d} = R_\mathrm{BLR} + TW + R_\gamma\cos\theta + c\tau_\mathrm{ob}/(1+z)$ and $TW = R_\mathrm{BLR}\sin\alpha\sin\theta$ (see Fig. 1*b*), and then

$$R_\gamma = \frac{R_\mathrm{BLR}(1 + \sin\alpha\sin\theta) + \frac{c\tau_\mathrm{ob}}{1+z}}{\frac{c}{v_\mathrm{d}} - \cos\theta}, \tag{6}$$

where α is the angle between AB and AT and varies from 0 to 2π. For a given source, i.e. given R_γ, R_BLR, v_d, θ and z, τ_ob varies with α, i.e. $\tau_\mathrm{ob} = \tau_\mathrm{ob}(\alpha)$. Calculating ensemble

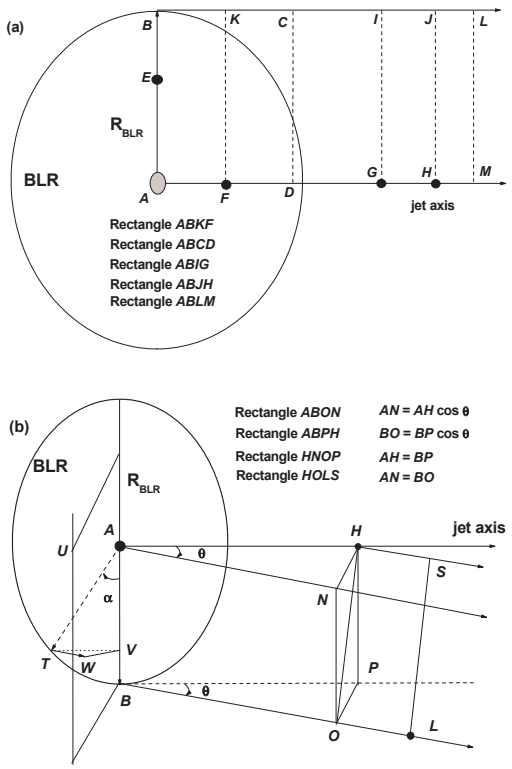

Figure 1. Sketch of the geometry assumed, and it is similar to that used in the reverberation mapping method of broad emission lines. $R_{\rm BLR}$ is the size of BLR. (a) the angle between the line of sight and the jet axis $\theta = 0$. (b) $\theta \neq 0$. The jet axis is perpendicular to the plane of BLR. (b) the planes ABU and $HNOP$ are perpendicular to the line of sight. $\because TV \perp AV$, $\therefore TV = AT\sin\alpha = R_{\rm BLR}\sin\alpha$. $\because TW \parallel BL$, $\therefore TW \perp WV$ and $TW \perp AV$. $TW \perp AV$ and $TV \perp AV$ give $WV \perp AV$. $\because TV \perp AV$ and $WV \perp AV$, $\therefore \angle TVW = \theta$. $\because \angle TVW = \theta$ and $\angle TWV = \pi/2$, $\therefore TW = TV\sin\theta = R_{\rm BLR}\sin\alpha\sin\theta$.

average over α in equation (6), we have

$$R_\gamma = \frac{R_{\rm BLR} + \frac{c\langle\tau_{\rm ob}\rangle}{1+z}}{\frac{c}{v_{\rm d}} - \cos\theta}, \qquad (7)$$

where $\langle\tau_{\rm ob}\rangle$ is the ensemble average of $\tau_{\rm ob}(\alpha)$ and is the measured time lag between the γ-ray and line light curves (and $\langle 1 + \sin\alpha\sin\theta\rangle = \int_0^{2\pi}(1+\sin\alpha\sin\theta){\rm d}\alpha/2\pi = 1$). It is obvious that equation (7) contains Cases A, B and C. As $\theta = 0$, equation (7) becomes equation (4). In the following sections, we will calculate R_γ based on equation (7).

3 APPLICATION TO 3C 273

3C 273 was first identified as a quasar at redshift $z = 0.158$ by Schmidt (1963). It is one of the best studied AGNs in all bands (see e.g. Lichti et al. 1995; von Montigny et al. 1997; Türler et al. 1999; Soldi et al. 2008). The database site[1] of 3C 273 provides a series of about 70 light curves as well as some spectra. The jet of 3C 273 is one-sided, with no signs of emission from the counterjet side (Unwin et al. 1985). The blue-bump of 3C 273 is thermal continuum emission from the inner accretion disc (Shields 1978). Fe Kα lines observed in 3C 273 were shown to be from an accretion disc around a supermassive black hole (Yaqoob & Serlemitsos 2000; Torres et al. 2003). If the assumptions in the method are correct, it is expected for 3C 273 that there should exist time lags between the broad lines from the BLR and the γ-rays from the relativistic jet.

3.1 Data of 3C 273

This paper makes use of the 3C 273 database hosted by the ISDC (Türler et al. 1999). This database is one of the most complete multi-wavelength databases currently available for one AGN. For 3C 273, the γ-ray light curves are very sparsely sampled and/or the error bars of γ-ray fluxes are also very large. Of course with *Fermi* taking data since June 2008 this is no longer the case (see e.g. Abdo et al. 2010b). However, the sampling over the dates of interest, and, in general over the timescales of interest is still sparse (see the line light curves in the following paragraphs). Thus it should be unreliable to employ the γ-ray light curves to estimate the time lags. Hence for these blazars lacking adequate γ-ray light curves, the synchrotron emission, especially the radio emission, could be used to derive the time lags relative to the broad lines. The synchrotron flares from the relativistic jet dominate energy output from radio to millimeter and extend up to the infrared–optical regimes (Robson et al. 1993; Türler, Courvoisier & Paltani 2000; Soldi et al. 2008). Radio light curves are better than millimeter ones in the samplings and the features of synchrotron flares. Gamma-ray detections correspond to rising radio fluxes (e.g. Ulrich, Maraschi & Urry 1997). Thus the radio light curves are adopted to be analyzed. Though the synchrotron flares extend up to the infrared–optical regimes, the flares are sparse (denoted by red color in the 3C 273 database). In the intervals among these flares, the infrared–optical light curves may be contaminated by other emission components. Thus it is expected that there should be no significant features in the cross correlation functions between the broad lines and the light curves. Considering that the synchrotron emission peaks around the infrared band for 3C 273 (see e.g. Ghisellini et al. 1998), the infrared light curves are also adopted to be analyzed and to test the expectation above. In the light curves adopted here, only good data (Flag>=0) are adopted.

Light curves of 5, 8, 15, 22 and 37 GHz are taken from the 3C 273 database, for these light curves have enough data (Türler et al. 1999). These radio light curves are presented in Fig. 2. There are four distinct outbursts in each radio light curve after $\sim$ 1980 (see Fig. 2). The data of 22 and 37 GHz are adopted from $\sim$ 1980, for observations are very sharply sampled before $\sim$ 1980 (see Fig. 2). From 1973 to 1978, there is a gap of 5 years without observations of 5 GHz. Considering the four distinct outbursts in each radio light curve, the data from $\sim$ 1980 are adopted for the light curve of 5 GHz. Also, the data from $\sim$ 1980 are adopted for the light curves of 8 and 15 GHz. The sampling rates of 5, 8, 15, 22 and 37 GHz are 29, 40, 40, 44 and 46 times per year for the adopted data, respectively.

Light curves of broad lines Hα, Hβ and Hγ are taken from Kaspi et al. (2000), and all the data in the light curves

[1] http://isdc.unige.ch/3c273/

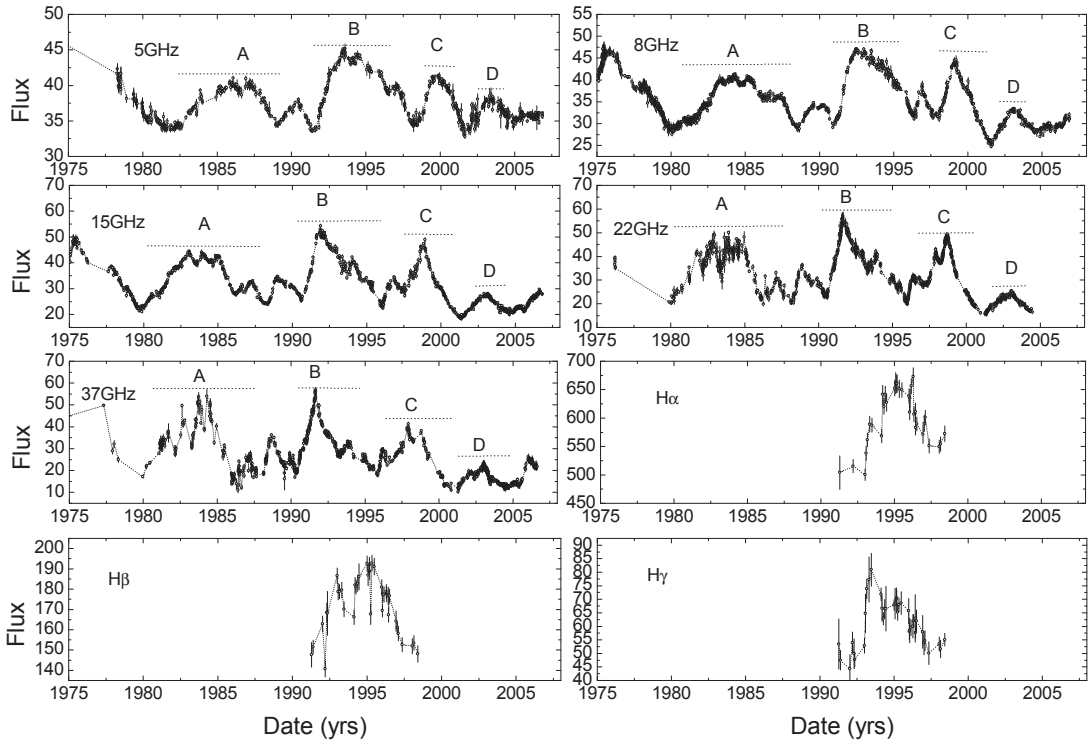

Figure 2. Light curves of the radio emission and the Balmer lines. The y-axis is in units of Jy. For lines, the y-axis is in units of 10^{-14} erg cm^{-2} s^{-1}. A, B, C and D denote the four distinct outbursts after $\sim$ 1980.

are adopted to calculate the time lags relative to the radio emission. The sampling rates of the lines are around 5 times per year. The line light curves are also presented in Fig. 2, wherein all the light curves show the same time interval. It can be seen in Fig. 2 that the line light curves are sharply sampled relative to the radio light curves adopted. Especially, there is only one data point in each of several valley-bottoms in the Hα and Hβ light curves, and the trend of variations can be changed if the points in these valley-bottoms are excluded from the Hα and Hβ light curves (see Fig. 2). The sharp samplings will affect the choice of analysis method for the cross correlation between the broad lines and the radio emission. The infrared light curves of J, H, K and L bands are also adopted from the 3C 273 database. The data before 1998 are adopted for the J, H and L light curves. The data before 2000 are adopted for the K light curve.

3.2 Analysis of time lags

Cross-correlation function (CCF) analysis is a standard technique in time series analysis for finding time lags between light curves at different wavelengths, and the definition of the CCF assumes that the light curves are uniformly sampled. However, in most cases the sampling is not uniform. The interpolated cross correlation function (ICCF) method of Gaskell & Peterson (1987) uses a linear interpolation scheme to determine the missing data in the light curves. On the other hand, the discrete correlation function (DCF; Edelson & Krolik 1988) can utilize a binning scheme to approximate the missing data. Apart from the ICCF and DCF, there is another method of estimating the CCF in the case of nonuniformly sampled light curves, the z-transformed discrete correlation function (ZDCF; Alexander 1997). The ZDCF is a binning type of method as an improvement of the DCF technique, but it has a notable feature in that the data are binned by equal population rather than equal bin width as in the DCF. It has been shown in practice that the ZDCF is more robust than the ICCF and the DCF when applied to sparsely and unequally sampled light curves (see e.g. Edelson et al. 1996; Giveon et al. 1999; Roy et al. 2000). Liu et al. (2008) analyzed the ZDCFs between unequally sampled light curves of AGNs, and they obtained inter-band time lags. In practice, the ZDCF is applicable and reliable to analyze the unequally sampled light curves. Thus the ZDCF will be calculated in the paper because of the sharp samplings of the Balmer lines.

In general, it seems to be true that the time lag is better characterized by the centroid $\tau_{\rm cent}$ of the DCF and the ICCF than by the peak value $\tau_{\rm peak}$, namely, the time lag where the linear correlation coefficient has its maximum value $r_{\rm max}$ (see e.g. Peterson et al. 2004, 2005). In both the DCF and the ICCF, $\tau_{\rm peak}$ is much less stable than $\tau_{\rm cent}$, but $\tau_{\rm peak}$ is much less stable in the DCF than in the ICCF (Peterson et al. 2005). Thus we prefer the time lag to be characterized by the centroid $\tau_{\rm cent}$ of the ZDCF. The centroid time lag $\tau_{\rm cent}$ is computed using all the points with correlation coefficients $r \geqslant 0.8 r_{\rm max}$ in the ZDCF bumps closer to the zero-lag (see Fig. 3). The calculated ZDCFs between the radio and broad-line light curves are presented in Fig. 3. The horizontal and vertical error bars in Fig. 3 represent the 68.3% confidence intervals in the time lags and the rele-

Table 1. Time lags between emission lines and radio emission. The sign of the time lag is defined as $\tau_{\rm cent} = t_{\rm radio} - t_{\rm line}$. Time lags are in units of yrs.

Lines	5 GHz	8 GHz	15 GHz	22 GHz	37 GHz
Hα	$-1.23^{+0.02}_{-0.07}$	$-1.99^{+0.06}_{-0.01}$	$-2.77^{+0.02}_{-0.08}$	$-3.14^{+0.02}_{-0.09}$	$-3.30^{+0.02}_{-0.08}$
Hβ	$-0.19^{+0.03}_{-0.09}$	$-1.06^{+0.08}_{-0.02}$	$-2.40^{+0.02}_{-0.07}$	$-2.27^{+0.03}_{-0.09}$	$-3.27^{+0.02}_{-0.08}$
Hγ	$-0.35^{+0.03}_{-0.09}$	$-1.13^{+0.07}_{-0.01}$	$-1.57^{+0.02}_{-0.07}$	$-1.82^{+0.02}_{-0.08}$	$-2.01^{+0.02}_{-0.07}$
Hα	$4.72^{+0.08}_{-0.02}$	$4.20^{+0.06}_{-0.02}$	$3.43^{+0.08}_{-0.02}$	$3.21^{+0.07}_{-0.02}$	$3.06^{+0.08}_{-0.03}$
Hβ	$4.31^{+0.07}_{-0.02}$	$4.13^{+0.07}_{-0.01}$	$3.72^{+0.07}_{-0.02}$	$3.45^{+0.07}_{-0.02}$	$3.26^{+0.09}_{-0.03}$
Hγ	$6.19^{+0.10}_{-0.04}$	$4.13^{+0.06}_{-0.01}$	$3.73^{+0.07}_{-0.02}$	$3.78^{+0.08}_{-0.03}$	$3.29^{+0.08}_{-0.03}$

vant correlation coefficients, respectively. The ZDCF bumps closer to the zero-lag have a good profile in Fig. 3. The measured time lags are listed in Table 1. The centroid $\tau_{\rm cent}$ is calculated by $\tau_{\rm cent} = \sum \tau(i) r(i) / \sum r(i)$, where $\tau(i)$ and $r(i)$ are the values of i-th data pair with $r \geqslant 0.8 r_{\rm max}$. The errors of $\tau_{\rm cent}$ are calculated by $\Delta\tau^{\pm}_{\rm cent} = \{\sum[\Delta\tau^{\pm}(i) r(i) + \tau(i)\Delta r^{\pm}(i)] \sum r(i) - \sum \tau(i) r(i) \sum \Delta r^{\pm}(i)\} / [\sum r(i)]^2$, where $\Delta\tau^{\pm}(i)$ and $\Delta r^{\pm}(i)$ are the relevant errors of $\tau(i)$ and $r(i)$, respectively.

Our results show two possibilities that the broad-line variations lag or lead the radio ones (see Fig. 3). The measured time lags are on the order of years (see Table 1). For a given line, the relevant time lags generally decrease as radio frequency increases from 5 to 37 GHz (see Table 1). The calculated ZDCFs between the infrared and Hα light curves are presented in Fig. 4 for illustration. For the ZDCFs in Fig. 4, there are no significant common features closer to the zero-lag. Also, there are no significant common features closer to the zero-lag for the ZDCFs of the Hβ and Hγ lines relative to the infrared emission. On the contrary, the ZDCFs in Fig. 3 have significant common features closer to the zero-lag. The absence of significant features tests the expectation in subsection 3.1. This test indicates that the infrared synchrotron emission does not dominate the energy output in the intervals between the synchrotron flares in the infrared–optical bands. The lag $\tau_{\rm ob}$ is the lag $\tau_{\rm cent}$ measured here. Hereafter, $\tau_{\rm cent}$ is equivalent to $\tau_{\rm ob}$ and $\langle\tau_{\rm ob}\rangle$.

3.3 Calculations

For 3C 273, Kaspi et al. (2000) determined the Hα, Hβ and Hγ lags τ relative to the optical continuum, and Paltani & Türler (2005) determined their lags relative to the UV continuum. The optical continuum is strongly contaminated by non-thermal emission, possibly related to the relativistic jet, and therefore it appears unsuitable for studying the lags between the ionizing continuum and the lines (Paltani, Courvoisier & Walter 1998). The Hα, Hβ and Hγ lags relative to the UV continuum are more reliable than those relative to the optical continuum (Paltani & Türler 2005). Thus we adopt the Hα, Hβ and Hγ lags determined by Paltani & Türler (2005). Here, the average of rest-frame lags of these lines, $\overline{\tau} = 2.70$ years, is adopted as a characteristic value of τ. Thus the BLR has a typical size of $R_{\rm BLR} = 2.70$ ly.

Simulations show that the relativistic jets can be driven from a region just outside the ergosphere of a Kerr black hole (see e.g. Meier, Koide & Uchida 2001; Koide et al. 2002; Koide 2004; Komissarov 2004; Semenov, Dyadechin & Punsly 2004). In most cases, the bulk velocity of jet $v_{\rm j}$ is close to the escape speed (Kudoh et al. 1998). The escape speed is around $0.9c$ near the ergosphere of the rapidly spinning black hole (Meier, Koide & Uchida 2001). Most supermassive black holes are spinning rapidly (Elvis, Risaliti & Zamorani 2002). Thus $v_{\rm j} \sim 0.9c$. If the disturbances in the cental engine are transported with the jet itself, $v_{\rm d} = v_{\rm j} \sim 0.9c$. Thus we would have $R_\gamma \sim 9 R_{\rm BLR}$ from equation (1).

For 3C 273, the jet has $v_{\rm j} = 0.95c$ and $\cos\theta = 0.95$ on 100 pc scales (Davis, Unwin, Muxlow 1991). The pc-scale jet was constrained to have $\theta < 15^\circ$ and the bulk Lorentz factor $\Gamma > 10$ (Unwin et al. 1985). The actual value of θ cannot be too small, unlike better aligned blazars, because it has a strong big blue bump (Shields 1978; Courvoisier 1998). Thus it is likely that θ be larger than 10°. The ratio of the jet to counterjet flux is $R = [(1 + v_{\rm j}\cos\theta/c)/(1 - v_{\rm j}\cos\theta/c)]^{3+\alpha}$ for discrete moving blobs (Lind & Blandford 1985). $R > 10^4$ was observed for 3C 273 and $v_{\rm j}$ can be up to $0.995c$ (see e.g. Georganopoulos et al. 2006). The observed spectral index $\alpha = 0.8$ (Unwin et al. 1985). It is obvious that $\theta \lesssim 21^\circ$ and $0.9c \leqslant v_{\rm j} \leqslant 0.995c$ are allowed by $R > 10^4$. The disturbances are transported from the central engine down the jet, and then it is possible that $v_{\rm d} = v_{\rm j} = 0.9$–$0.995c$ and $\theta = 12^\circ$–21°. For a given line, the relevant time lags generally decrease as radio frequency increases from 5 to 37 GHz (see Table 1). We adopt the measured time lags of the lines relative to the 37 GHz emission. The negative lags have an average of $\overline{\tau}^{-}_{\rm ob} = -2.86$ years. The positive lags have an average of $\overline{\tau}^{+}_{\rm ob} = 3.20$ years. There is no zero-lag. In the following calculations, $v_{\rm d} = 0.9$–$0.995c$ and $\theta = 12^\circ$–21° are adopted, and these values estimated from $\tau_{\rm ob}$ are denoted by $R_{\rm radio}$.

From $\overline{\tau}^{-}_{\rm ob} = -2.86$ years, $R_{\rm BLR} = 2.70$ ly, $v_{\rm d} = 0.9$–$0.995c$, $\theta = 12^\circ$–21° and equation (7), we can obtain the radio emitting position $R_{\rm radio} = 0.40$–2.62 pc (Case B). The typical size of $R_{\rm BLR} = 2.70$ ly $= 0.83$ pc is within the range of $R_{\rm radio}$ estimated in Case B. The radio emitting regions in Case B are at distances of pc-scale from the central engine and are around the BLR, i.e. likely inside the BLR, co-located with the BLR or outside the BLR. From $\overline{\tau}^{+}_{\rm ob} = 3.20$ years, $R_{\rm BLR} = 2.70$ ly, $v_{\rm d} = 0.9$–$0.995c$, $\theta = 12^\circ$–21° and equation (7), we can obtain $R_{\rm radio} = 9.43$–62.31 pc (Case C). The estimated sizes are much larger than the typical size of $R_{\rm BLR} = 0.83$ pc. The radio emitting regions in Case C are at distances of tens of pc from the central black hole and are far away from the BLR.

Kovalev et al. (2009) identified the pc-scale radio core as a likely location for both the γ-ray and radio flares.

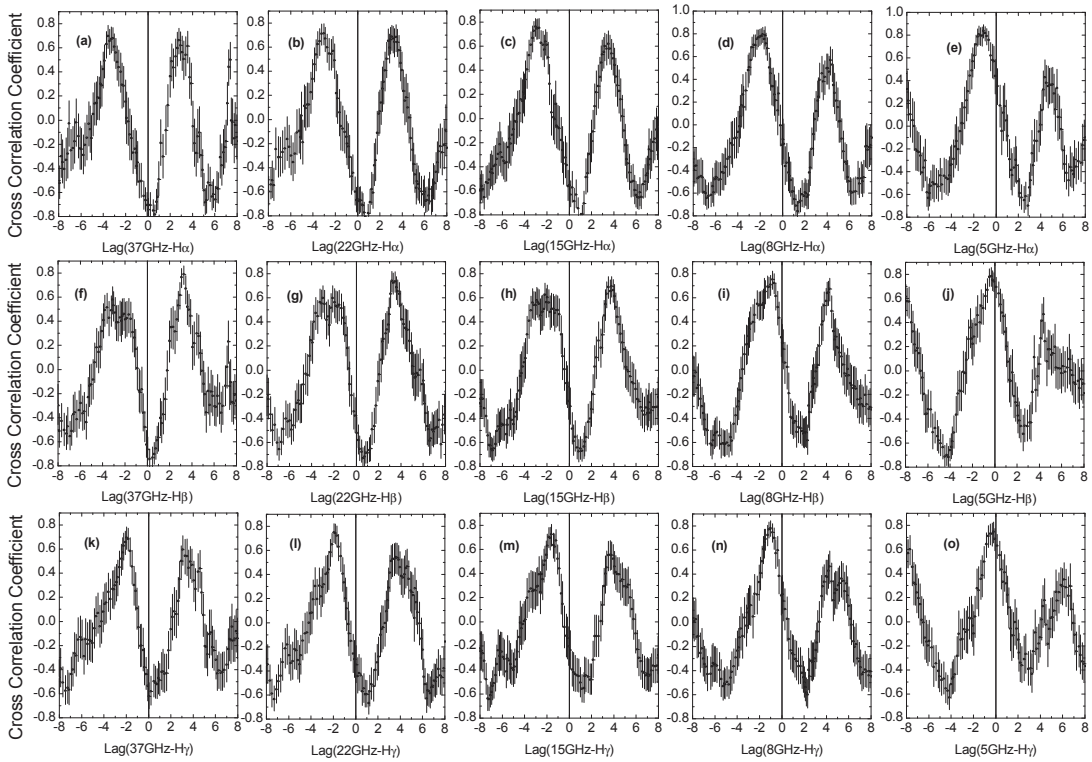

Figure 3. ZDCF between Hα and (*a*) 37, (*b*) 22, (*c*) 15, (*d*) 8 and (*e*) 5 GHz; ZDCF between Hβ and (*f*) 37, (*g*) 22, (*h*) 15, (*i*) 8 and (*j*) 5 GHz; ZDCF between Hγ and (*k*) 37, (*l*) 22, (*m*) 15, (*n*) 8 and (*o*) 5 GHz. The x-axis is in units of yrs.

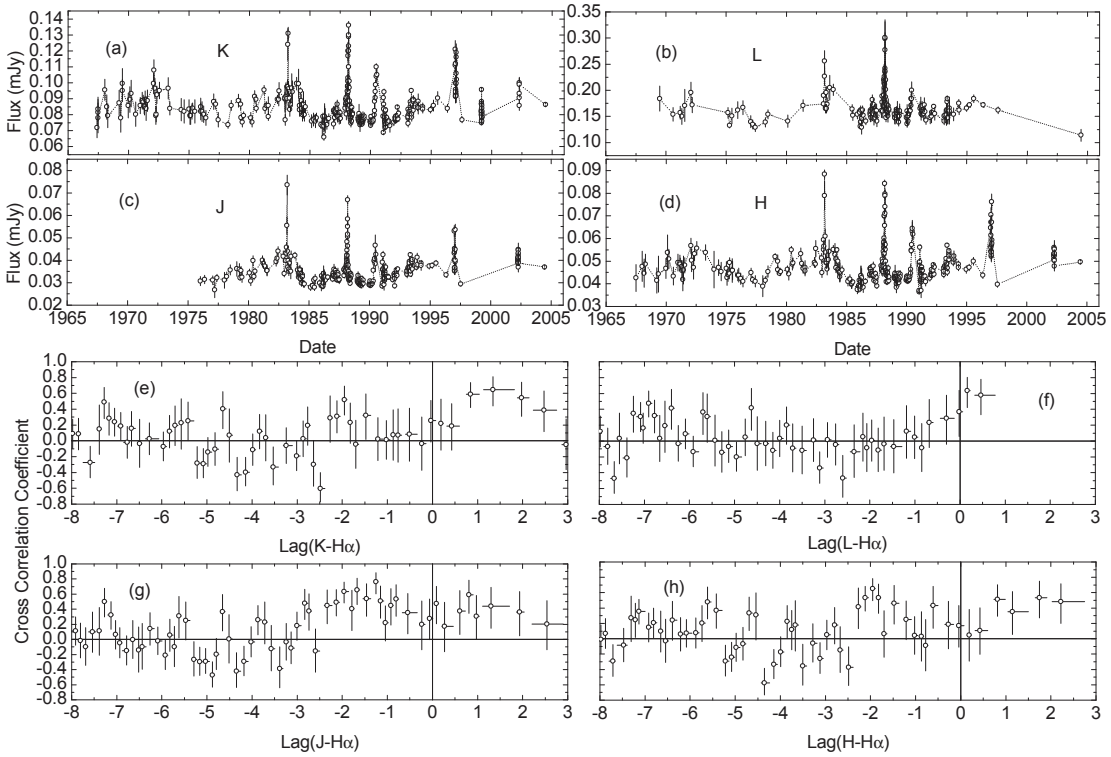

Figure 4. Light curves of infrared emission in (*a*) K, (*b*) L, (*c*) J and (*d*) H bands. ZDCF between Hα and (*e*) K, (*f*) L, (*g*) J and (*h*) H bands. The x-axis is in units of yrs.

Jorstad et al. (2001) concluded that both the radio and γ-ray events are originating from the same region of a relativistic jet. In 1990s, it is commonly thought that the γ-rays are produced in the jet, but closer to the central engine than the radio emission (see e.g. Dermer & Schlickeiser 1994). Thus it is expected that $R_\gamma \lesssim R_{\rm radio}$. The constraint of $R_\gamma \lesssim R_{\rm radio}$ is allowed by the recent flares of 3C 279 observed by *Fermi* and in a multi-wavelength campaign (Abdo et al. 2010d), where radio light curves from 5 to 230 GHz fail to show prominent variations during either the November 2008 or the February 2009 γ-ray flares (or anytime in between). For Case B, $R_\gamma \lesssim 0.40$–2.62 pc for $v_{\rm d} = 0.9$–$0.995c$ and $\theta = 12°$–$21°$. For Case A, the zero-lag position $R_\gamma = 4.67$–30.81 pc, which is far away from the BLR. For Case C, $R_\gamma \lesssim 9.43$–62.31 pc. Also, $R_\gamma > 4.67$–30.81 pc for the positive lags in Case C. Thus for Case C we have 4.67–$30.81 < R_\gamma \lesssim 9.43$–$62.31$ pc for $v_{\rm d} = 0.9$–$0.995c$ and $\theta = 12°$–$21°$. The dependence of R_γ and $R_{\rm radio}$ on $v_{\rm d}$ and θ is presented in Fig. 5 (see three-dimensional plots). R_γ and $R_{\rm radio}$ increase as $v_{\rm d}$ increases, but decrease as θ increases. The uncertainties of $v_{\rm d}$ and θ result in the larger intervals of R_γ and $R_{\rm radio}$. For better representing intervals of R_γ, the sections of the three-dimensional plots at $\cos\theta = 0.95$ are also plotted in Fig. 5 (see the bottom panel). For Case B, $R_\gamma \lesssim R_{\rm radio} = 0.44$–$1.28$ pc for $v_{\rm d} = 0.9$–$0.995c$ and $\cos\theta = 0.95$. These R_γ marginally satisfy $R_\gamma \lesssim R_{\rm BLR}$. For Case C, we have 5.15–$15.08 < R_\gamma \lesssim 10.40$–$30.45$ pc.

It is possible that there is a special point D within segment AG (see Fig. 1*a*). As the ionizing photons travel from point A to B, the disturbances travel from A to D, i.e. $R_\gamma = AD$. Thus we have $R_\gamma/v_{\rm d} = R_{\rm BLR}/c$, and then

$$R_\gamma = \frac{R_{\rm BLR}}{c} v_{\rm d}. \tag{8}$$

In this case, the γ-rays will lead the lines. Combing equations (7) and (8), we have

$$R_\gamma = -\frac{c\langle\tau_{\rm ob}\rangle}{1+z}\frac{1}{\cos\theta}. \tag{9}$$

In this special case (hereafter Case D), $R_\gamma \lesssim R_{\rm BLR}$ is expected from equation (8). From $\overline{\tau}_{\rm ob} = -2.86$ years, $\theta = 12°$–$21°$ and equation (9), we have $R_\gamma \lesssim R_{\rm radio} = 0.77$–$0.81$ pc. These estimated R_γ and $R_{\rm BLR} = 0.83$ pc satisfy $R_\gamma \lesssim R_{\rm BLR}$. This tests the correctness of $R_\gamma \lesssim R_{\rm BLR}$ expected from equation (8). This test confirms the reliability of the time lags estimated by the ZDCF method. Those estimated $R_{\rm radio}$ in Case B contain these $R_{\rm radio}$ estimated in Case D. Thus Case D is a special Case B, and it is possible and reasonable. Combining equations (7) and (8), one can also obtain

$$R_{\rm BLR} = -\frac{c\langle\tau_{\rm ob}\rangle}{1+z}\frac{c}{v_{\rm d}}\frac{1}{\cos\theta}. \tag{10}$$

From $\overline{\tau}_{\rm ob} = -2.86$ years, $v_{\rm d} = 0.9$–$0.995c$, $\theta = 12°$–$21°$ and equation (10), we have $R_{\rm BLR} = 0.77$–0.90 pc. These estimated values contain the typical size of $R_{\rm BLR} = 0.83$ pc. This confirms the reliability of the time lags estimated by the ZDCF method.

4 DISCUSSION AND CONCLUSIONS

The positions of γ-ray–emitting regions are still an open and controversial issue in the researches on blazars. Based

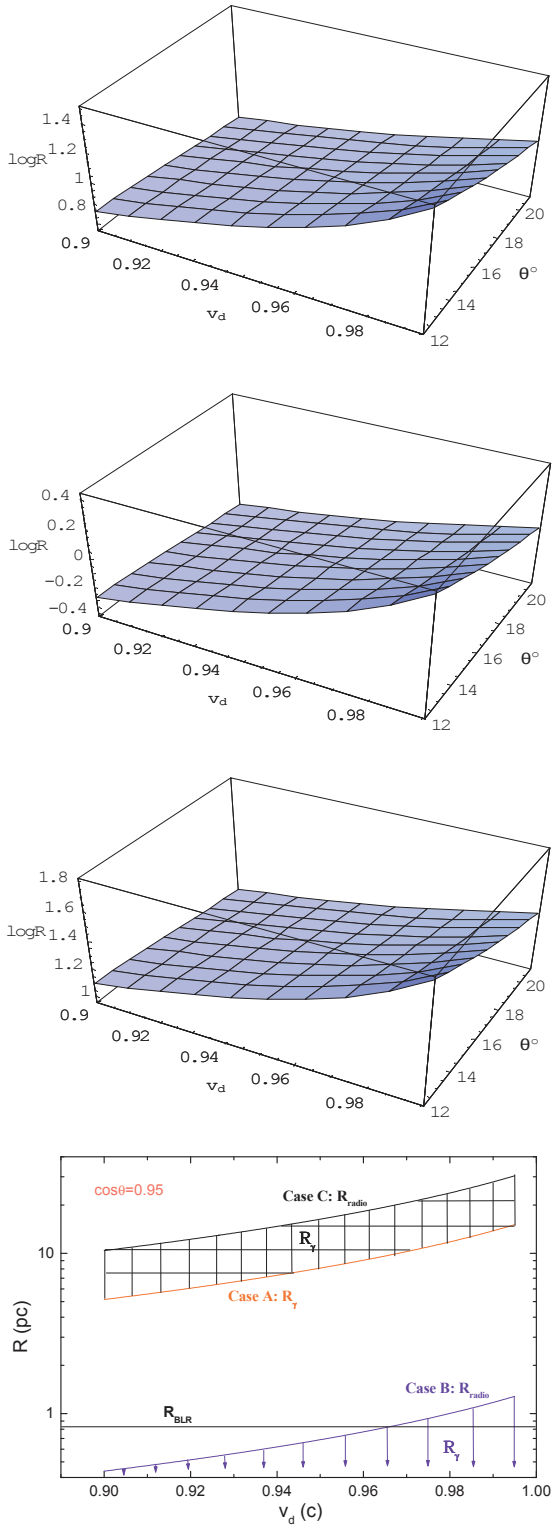

Figure 5. Dependence of distance R on $v_{\rm d}$ and θ. From the top down, the first three panels correspond to Cases A, B and C, respectively. The x, y and z-axes are $v_{\rm d}$ in units of c, θ in units of degree and $\log R$ in units of pc, respectively. The first three panels represent dependence of R on $v_{\rm d}$ and θ. The bottom panel represents dependence of R on $v_{\rm d}$ in case of $\cos\theta = 0.95$, where the gridding area represents the allowed interval of R_γ in Case C. The arrows represent the upper limit of R_γ in Case B.

on the method proposed in section 2, we attempt to locate the emitting positions of γ-rays within the second bumps in the broad-band SEDs of blazars. In our previous works (Liu & Bai 2006; Liu, Bai & Ma 2008; Bai, Liu & Ma 2009), the internal absorption for 10 GeV–1 TeV γ-rays were used to constrain R_γ, independent of how the γ-rays are produced. Here, we try to locate R_γ, independent of the energies of γ-rays from the SSC and EC processes. We find two emitting regions, the inner one at sub-pc–pc scales from the central black hole and the outer one around tens of pc scales. The outer one satisfies $R_\gamma \gg R_{\rm BLR}$ (Case C). The inner one in Case D satisfies $R_\gamma \lesssim R_{\rm BLR}$. The inner one in Case B mostly satisfies $R_\gamma \lesssim R_{\rm BLR}$. At the same time, the inner one in Case B partly satisfies $R_\gamma > R_{\rm BLR}$, i.e. $R_{\rm BLR} < R_\gamma \lesssim$ 2.62 pc.

It was suggested $R_\gamma \lesssim R_{\rm BLR}$ (Ghisellini & Madau 1996). Georganopoulos, Kirk & Mastichiadis (2001) argued $R_\gamma \lesssim R_{\rm BLR}$ for powerful blazars. Tavecchio & Mazin (2009) assumed $R_\gamma < R_{\rm BLR}$ for the VHE γ-rays in 3C 279. Liu, Bai & Ma (2008) and Bai, Liu & Ma (2009) suggested that R_γ is within the BLR for 3C 279. Ghisellini et al. (2010) modelled the SEDs of bright *Fermi* blazars, and they found that the position of the jet dissipation region $R_{\rm diss}$ is smaller than $R_{\rm BLR}$ for 53 out of 57 FSRQs. However, $R_{\rm diss} > R_{\rm BLR}$ for BL Lacs. They used $R_{\rm BLR} = 10^{17} L_{\rm d,45}^{1/2}$ cm to estimate $R_{\rm BLR}$ for BL Lacs and FSRQs, where $L_{\rm d,45}$ is accretion disc luminosity in units of 10^{45} erg s^{-1}. It is appropriate to use $R_{\rm BLR} = 10^{17} L_{\rm d,45}^{1/2}$ cm to estimate $R_{\rm BLR}$ for FSRQs, but not for BL Lacs because this relation is derived from the type 1 AGNs. Thus it should be reliable that $R_{\rm diss} < R_{\rm BLR}$ for blazars. If the jet dissipation region is equivalent to the γ-ray–emitting region, $R_{\rm diss} < R_{\rm BLR}$ is equivalent to $R_\gamma < R_{\rm BLR}$. For 3C 273, $R_{\rm diss} < R_{\rm BLR}$ (Ghisellini et al. 2010). These previous findings are consistent with our results of $R_\gamma \lesssim R_{\rm BLR}$ obtained in Cases B and D. It was also argued $R_\gamma > R_{\rm BLR}$ (Lindfors, Valtaoja & Türler 2005; Sokolov & Marscher 2005). This is marginally consistent with $R_{\rm BLR} < R_\gamma \lesssim 2.62$ pc obtained in Case B. These agreements confirm the reliability of the method and assumptions.

Böttcher (2008) suggested for 3C 279 that $R_\gamma \gg R_{\rm BLR}$ for VHE γ-rays. It is recently advanced that the bulk of the γ-rays is produced in regions of the jet at distances of tens of pc from the central black hole (e.g. Sikora, Moderski & Madejski 2008; Marscher et al. 2010). Bai & Lee (2001) predicted the existence of large scale synchrotron X-ray jets in radio-loud AGNs, especially, the X-ray jets are bright on 10 kpc scales in most red blazars and red blazar-like radio galaxies. According to their predictions, the large scale synchrotron X-ray jets can produce VHE γ-rays by the SSC process. Zhang et al. (2009, 2010) predicted the hot spots in lobes and the knots in jets to be possible GeV–TeV emitters. *Fermi*/LAT may resolve the large scale γ-ray emitters than the nuclear emitters. These previous findings support $R_\gamma \gg R_{\rm BLR}$ as we obtain in Case C. Also, $R_\gamma \gg R_{\rm BLR}$ in Case C is not inconsistent with $R_\gamma > R_{\rm BLR}$ of Lindfors, Valtaoja & Türler (2005) and Sokolov & Marscher (2005). These confirm the reliability of our results.

Our previous works are applicable to the γ-rays emitted from the regions in powerful blazars, where R_γ is not much larger than $R_{\rm BLR}$ (Liu & Bai 2006; Liu, Bai & Ma 2008; Bai, Liu & Ma 2009). The method proposed here can locate R_γ in the jet. The inner emitting regions with $R_\gamma \lesssim R_{\rm BLR}$ are likely the major contributor of the γ-rays below 10 GeV, for that the γ-rays above 10 GeV are subject to the photon-photon absorption due to the dense external soft photons at the inner regions (e.g. Liu & Bai 2006; Liu, Bai & Ma 2008; Bai, Liu & Ma 2009). The outer emitting regions with $R_\gamma \gg R_{\rm BLR}$ are likely the major contributor of the γ-rays above 10 GeV, for that these γ-rays are not subject to the photon-photon absorption due to the thin external soft photons at the outer regions. For these possible γ-ray emitters at large scales of kpc–Mpc (Bai & Lee 2001; Zhang et al. 2009, 2010), our works are not applicable.

The most prominent features on VLBI images of jets in radio-loud AGNs are the radio core and bright knots in the jet (Jorstad et al. 2007). Kovalev et al. (2009) investigated the relation between AGN γ-ray emission and pc-scale radio jets. They identified the pc-scale radio core as a likely location for both the γ-ray and radio flares. A few hundreds of Schwarzschild radii, sub-pc-scale, is the preferred jet position where most of the dissipation occurs (Ghisellini & Tavecchio 2009; Ghisellini, Tavecchio & Ghirlanda 2009; Ghisellini et al. 2010). Sikora et al. (2009) suggested that the blazar emission zone is located at pc-scale distances from the nucleus. Ghisellini & Madau (1996) suggested that R_γ is at sub-pc scales. Blandford & Levinson (1995) also suggested a sub-pc γ-ray–emitting region from the central black hole. These previous findings support R_γ at sub-pc–pc scales. These R_γ of sub-pc–pc scales are consistent with those R_γ obtained in Cases B and D. These sub-pc–pc scale $R_{\rm radio}$ obtained in Cases B and D are also consistent with the previous findings of the blazar emission zone and the dissipation zone. These agreements confirm the reliability of our results.

It is recently advanced that the bulk of the γ-rays is generated in regions of the jet at distances of tens of pc from the central black hole (e.g. Sikora, Moderski & Madejski 2008; Marscher et al. 2010). For Case C, we obtain the outer emitting regions of 4.67–30.81 $< R_\gamma \lesssim$ 9.43–62.31 pc and $R_{\rm radio}$ = 9.43–62.31 pc. These outer emitting regions are comparable to the γ-ray–emitting regions at distances of tens of pc. Tavecchio et al. (2010) found evidence of variability on timescales of few hours from the 1.5 years *Fermi*/LAT light curves of FSRQs 3C 454.3 and PKS 1510-089. They concluded that significant variability on such short timescales disfavor the scenario in which the bulk of the γ-rays is produced at distances of tens of pc (e.g. Sikora, Moderski & Madejski 2008; Marscher et al. 2010). The previous researches show that there are two possible γ-ray–emitting regions, one inside or around the BLR and the other outside the BLR. This paper gives the same results. However, the method cannot discriminate between positive lags and negative lags on observational grounds alone (at least not with the current data), and the application discussed in the paper does not distinguish between the two proposed scenarios. We expect this situation to change with future data, perhaps longer line light curves, such as 10–15 years. The longer line light curves could give stronger constraints on the coupling of the radio light curves with the line ones.

For a given line, the relevant time lags generally de-

crease as radio frequency increases from 5 to 37 GHz. The trend is likely from the radiative cooling of relativistic electrons. Bai & Lee (2003) deduced the synchrotron time lag formula (see equation 9 therein). This formula can be expressed as in the observer's frame

$$\tau_{\rm lag}^{\rm ob}({\rm yrs}) = 1492.6\frac{\sqrt{1+{\rm z}}{\rm B}^{-3/2}}{\sqrt{\delta}(1+{\rm D})}\left(\nu_{\rm H}^{-1/2}-\nu_{\rm L}^{-1/2}\right), \quad (11)$$

where D is the "Compton dominance" (see e.g. Ghisellini et al. 1998), B is the magnetic field strength in units of gauss, δ is the Doppler factor, and $\nu_{\rm H}$ and $\nu_{\rm L}$ in units of GHz are high and low frequencies in the observer's frame, respectively. For 3C 273, Ghisellini et al. (1998) obtained $B = 8.9$ G and $\delta = 6.5$. Because the radio light curves used to calculate the ZDCFs span more than 20 years and the line light curves span about 7.5 years, it is better to derive D by using the ratio of synchrotron to γ-ray average luminosity. D is of the order of magnitudes of 1 (Türler et al. 1999). We can obtain $\tau_{\rm lag}^{\rm ob}({\rm yrs}) = 12(\nu_{\rm H}^{-1/2}-\nu_{\rm L}^{-1/2})$ if $D = 1$ is adopted. The total cooling of both synchrotron and γ-ray emission can lead to $\tau_{\rm lag}^{\rm ob}({\rm yrs}) = 6(\nu_{\rm H}^{-1/2}-\nu_{\rm L}^{-1/2})$. We calculate the ZDCFs and time lags between the light curves of 5, 8, 15, 22 and 37 GHz. The high frequency variations lead the low frequency ones. The measured time lags $\tau_{\rm lag}^{\rm ob}$ and the relevant frequency differences $\nu_{\rm H}^{-1/2}-\nu_{\rm L}^{-1/2}$ are presented in Fig. 6. The observational data are well consistent with the prediction of $\tau_{\rm lag}^{\rm ob} = 6(\nu_{\rm H}^{-1/2}-\nu_{\rm L}^{-1/2})$ (see Fig. 6). This agreement confirms the origin of radiative cooling for the time lags between the radio light curves used here. Pyatunina et al. (2006, 2007) also found frequency-dependent time delays for strong outbursts in several other blazars. In Fig. 7, we compare the lags $\tau_{\rm lag}^{\rm ob}$ with the differences of $\Delta\tau_{\rm cent}$ between $\tau_{\rm cent}$ listed in Table 1. The line of $\Delta\tau_{\rm cent} = \tau_{\rm lag}^{\rm ob}$ is consistent with the measured data points (see Fig. 7). This agreement confirms that the trend, i.e. the lags for a given line generally decrease as radio frequency increases, most likely results from the radiative cooling of relativistic electrons.

In addition, there is another possibility that lower frequencies probe larger radii in the jet, as synchrotron self-absorption is important for increasingly high radius with decreasing radio frequency. The synchrotron self-absorption coefficient α_ν is $\alpha_\nu \propto \nu^{-(n+4)/2}N_{\rm e}$, where $N_{\rm e}$ is the electron density and n is the electron distribution index. For a homogeneous blob with a radius of r, the synchrotron self-absorption optical depth τ_ν is $\tau_\nu = r\alpha_\nu \propto r\nu^{-(n+4)/2}N_{\rm e} \propto r\nu^{-(n+4)/2}/r^3 = \nu^{-(n+4)/2}/r^2$. Thus the radio frequency ν can probe the radius r that scales as $r \propto \nu^{-(n+4)/4}$. Hence, lower frequencies probe larger radii in the jet due to the synchrotron self-absorption. The higher frequencies will escape earlier from the blob and later the lower ones as the blob expands. Thus the lower frequencies lag the higher ones, and the relevant time lags $\tau_{\rm lag}$ are related to frequencies. The difference in lags listed in Table 1 could originate from the synchrotron self-absorption, and it scales with frequencies as $\tau_{\rm lag} \propto r_{\rm L} - r_{\rm H} \propto \nu_{\rm L}^{-(1+n/4)} - \nu_{\rm H}^{-(1+n/4)}$. The dependence of $\tau_{\rm lag}$ on frequencies is different from that of equation (11).

It seems possible to infer $R_{\rm radio}$ based on the time lags of the radio synchrotron emission relative to the UV continuum used by Paltani & Türler (2005). This approach seems more direct than based on the lags of the broad lines relative to the radio emission. We calculate the ZDCF between the light curves of the UV continuum and the 37 GHz emission. There is only a little bump closer to the zero-lag for the ZDCF and the little bump has $r_{\rm max} = 0.32 \pm 0.06$. In the ZDCFs between the Balmer lines and this radio emission, the bumps used to calculate $\tau_{\rm cent}$ have $r_{\rm max} = 0.6$–0.7 that are much higher than $r_{\rm max} = 0.32 \pm 0.06$. This indicates that the correlation of the UV continuum with this radio emission is much weaker than the Balmer lines with this radio emission. For 22, 15, 8 and 5 GHz, there are the same cases as in 37 GHz. The UV continuum is regarded as the ionizing continuum that drives the broad lines through the photoionization process. Thus it is expected that the correlation of the UV continuum with the radio synchrotron emission should be more significant than the broad lines with the radio emission. However, this expectation is contrary to the measurements in the paper. This disagreement indicates that the UV continuum is likely not the real ionizing continuum. Paltani & Türler (2005) argued that the UV continuum is much closer to the ionizing continuum than the optical continuum used by Kaspi et al. (2000). That is, the UV continuum is still not the real ionizing continuum. Thus

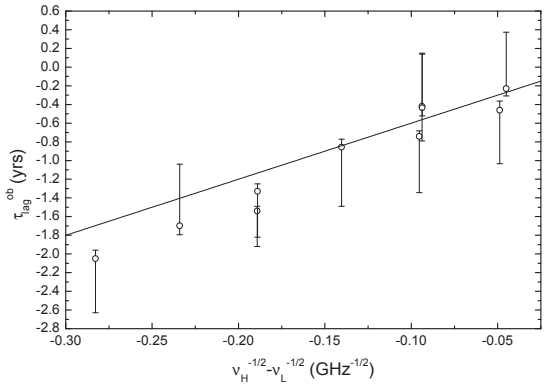

Figure 6. Relation of time lags $\tau_{\rm lag}^{\rm ob} = t_{\nu_{\rm H}} - t_{\nu_{\rm L}}$ and frequency differences $\nu_{\rm H}^{-1/2} - \nu_{\rm L}^{-1/2}$ between 37, 22, 15, 8 and 5 GHz. Solid line is the expectation from the radiative cooling.

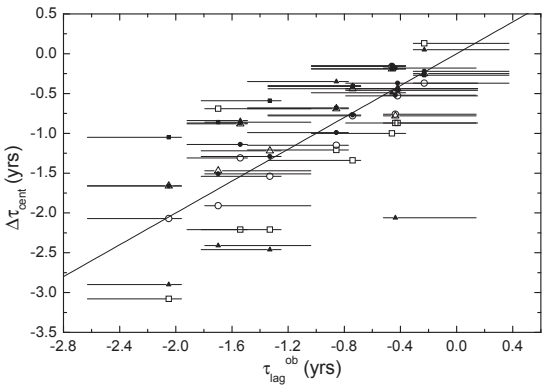

Figure 7. $\Delta\tau_{\rm cent}$ vs $\tau_{\rm lag}^{\rm ob}$. Circles present Hα, squares Hβ and triangles Hγ. Open symbols present the negative lags and fulled symbols the positive lags in Table 1. Solid line is $\Delta\tau_{\rm cent} = \tau_{\rm lag}^{\rm ob}$.

it is more reliable to derive $R_{\rm radio}$ from the lags of the broad lines relative to the radio emission than from those of the radio emission relative to the UV continuum.

The relativistic shortening of variation timescales seems to have significant effect on the the estimates of time lags. The correlation between the ejection epochs of jet components (superluminal radio knots) and the dips in the X-ray emission was interpreted as accretion of the X-ray–emitting gas in the inner accretion disc into the central black holes and ejection of a portion of the infalling material into the jet (see e.g. Marscher et al. 2002). An instability in the accretion flow causing a section of the inner disc break off. Part of this section is drawn into the event horizon of the central black hole but with considerable material and energy ejected down the jet. The loss of this section of the inner disc causes a decrease in the soft X-ray flux, which is observed as a dip. This disturbance from the inner accretion disc to the jet is observed as the ejection of a superluminal radio knot from the radio core of the jet. The dips in the X-ray flux represent the onset of the disturbances in the central engine. The knots represent the synchrotron emission of the transported disturbances at the sites of ejections. Hence, the intervals between the epochs of the dips $\Delta t_{\rm dip}$ represent those between the disturbances in the central engine. The intervals between the ejection epochs of knots $\Delta t_{\rm knot}$ result from the disturbances in the central engine. In the radio galaxy 3C 120, it was found that there are 13 ejection epochs of radio knots with the corresponding dips in the X-ray flux (Chaterjee et al. 2009). The ejection epochs $t_{\rm knot}$ and the corresponding epochs of dips $t_{\rm dip}$ have a good correlation with $t_{\rm knot} = t_{\rm dip} + 0.19$. For the 13 data pairs of $t_{\rm knot}$ and $t_{\rm dip}$, $\Delta t_{\rm knot}$ and $\Delta t_{\rm dip}$ between data pairs are equal to each other within the uncertainties, i.e. $\Delta t_{\rm knot} = \Delta t_{\rm dip}$. The correlation of $t_{\rm knot} = t_{\rm dip} + 0.19$ also gives $\Delta t_{\rm knot} = \Delta t_{\rm dip}$. For the ejections of knots in 3C 120, there are the relevant local peaks in synchrotron emission flux from the jet (Chaterjee et al. 2009; Tavares et al. 2010). The intervals between the epochs of peaks $\Delta t_{\rm peak}$ are equal to $\Delta t_{\rm knot}$ of the relevant ejections within the uncertainties, i.e. $\Delta t_{\rm peak} = \Delta t_{\rm knot}$. Combing $\Delta t_{\rm knot} = \Delta t_{\rm dip}$ and $\Delta t_{\rm peak} = \Delta t_{\rm knot}$, we have $\Delta t_{\rm peak} = \Delta t_{\rm dip}$. The intervals $\Delta t_{\rm peak}$ are measured by the light curves of beamed synchrotron emission from the jet. The intervals $\Delta t_{\rm dip}$ are measured by the light curves of un-beamed emission from a disc–corona system (Chaterjee et al. 2009). These intervals $\Delta t_{\rm peak}$ and $\Delta t_{\rm dip}$ are generated by the same disturbances from the disc to the jet. Thus it is likely that the relativistic effects on the time lags between them are negligible as both variations of the beamed synchrotron emission from the jet and the un-beamed emission from the disc–corona system are mainly generated by the same disturbances from the disc to the jet. In fact, the DCF method was employed to search the time lag between the X-ray and the 37 GHz variations in 3C 120, and one anti-correlation was found with the X-ray leading the radio variations by 120 ± 30 days (Chaterjee et al. 2009). By the DCF method, Courvoisier et al. (1990) obtained for 3C 273 that the UV light curve leads the radio emission by a few months. Based on this lag, Courvoisier (1998) showed that the radio emission is located some 4 light years from the central source along the jet. Though the relativistic effects are not considered in these DCFs used to estimate the time lags of the radio emission relative to the un-beamed emission of the UV and the X-rays, receivable results are obtained in these works. By analogy, it is likely that the relativistic effects would not have significant influence on these ZDCFs between the radio emission and the broad-line light curves used in the paper. Hence, the inferred time lags from these ZDCFs should not be affected by the relativistic effects very significantly.

For testing the correctness of the time lags obtained by these ZDCFs, we compare the 37 GHz light curve with the broad-line light curves moved horizontally and vertically (see Fig. 8). For the positive lags adopted, the line light curves are moved right by 2.8 years for Hα, 3.5 years for Hβ and 4.0 years for Hγ. For the negative lags adopted, the line light curves are moved left by 3.3 years for Hα, 3.2 years for Hβ and 2.0 years for Hγ. These moved line light curves are basically co-varied with the radio light curve (see Fig. 8). The relation of $\Delta t_{\rm peak} = \Delta t_{\rm dip}$ in 3C 120 also indicates that they should have similar observed timescales if both variations of the beamed synchrotron emission from the jet and the un-beamed emission from the disc–corona system are mainly generated by the same disturbances from the disc to the jet. These moved times are basically consistent with those time lags listed in Table 1. The averages of these moved times for the positive and negative lags are consistent with $\overline{\tau}^{+}_{\rm ob} = 3.20$ years and $|\overline{\tau}^{-}_{\rm ob}| = 2.86$ years obtained in these ZDCFs, respectively. The local peaks in the radio light curve basically have the corresponding ones in the moved line light curves. These indicate that the relativistic effects would not have significant influence on the estimates of time lags. The disturbances in the accretion flow passing through the sites of the central ionizing continuum could be imprinted on the ionizing continuum, the broad emission lines and the disc-jet system. In order to simulate the influence of the disturbances on the synchrotron emission from the jet, the transporting process of the disturbances from the disc to the jet should first be simulated by general relativistic magnetohydrodynamics (GRMHD, see e.g. Komissarov 2002; McKinney 2006). The light curves of broad emission lines could be simulated by the photoionization code CLOUDY (Ferland et al. 1998). The GRMHD simulations might give the site of radio synchrotron emission, and then it will be easy to estimate the time lags of the radio emission relative to the broad lines. Also, time lags can be derived from those ZDCFs between the simulated light curves of radio and line emission. Comparing the two kinds of time lags from simulations should determine whether or not the relativistic effects are considered in the ZDCF analysis between one beamed emission and one un-beamed emission due to the same disturbances. These simulations are out of the scope of this paper.

In the paper, we propose a new method to derive the γ-ray–emitting position R_γ from the time lags $\tau_{\rm ob}$ of the γ-ray emission relative to the broad lines (see Fig. 1). The method is also applicable to lower energy bands, such as radio emission. R_γ depends on four parameters $R_{\rm BLR}$, $\upsilon_{\rm d}$, $\tau_{\rm ob}$ and θ. As $\tau_{\rm ob} = 0$, $\tau_{\rm ob} < 0$ and $\tau_{\rm ob} > 0$ (Cases A, B and C), the broad lines zero-lag, lag and lead the γ-rays, respectively. All cases are unified into equation (7). The method is applied to FSRQ 3C 273. Because the γ-ray light curves are very sparsely sampled for 3C 273, it should be unreliable to employ them to estimate the time lags. Fortunately, it was

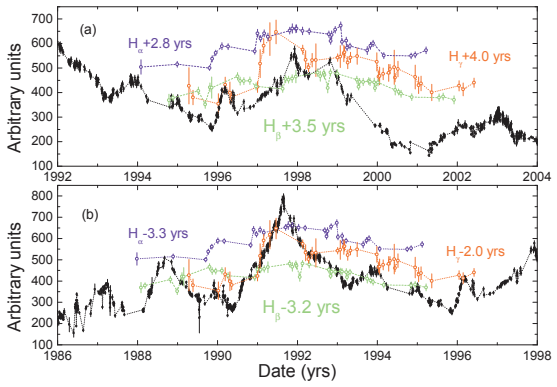

Figure 8. The 37 GHz light curve versus the Hα, Hβ and Hγ line light curves moved horizontally and vertically. (*a*) the positive lags: moved right. (*b*) the negative lags: moved left.

suggested that $R_\gamma \lesssim R_{\rm radio}$ (Dermer & Schlickeiser 1994; Jorstad et al. 2001; Kovalev et al. 2009; Abdo et al. 2010d). Thus R_γ could be constrained by $R_{\rm radio}$ derived from the lags of the radio emission relative to the broad lines. The ZDCF method is used to analyze the correlations of the radio and infrared emission with the broad lines Hα, Hβ and Hγ. The broad lines lag or lead the 5, 8, 15, 22 and 37 GHz emission (see Fig. 3). However, there is a lack of correlation between the infrared emission and the broad lines (see Fig. 4). The measured lags are on the order of years (see Table 1). The measured lags for a given line generally decrease as radio frequency increases (see Table 1). This trend most likely results from the radiative cooling of relativistic electrons (see Fig. 7). The measured negative lags have an average of $\overline{\tau}^-_{\rm cent} = -2.86$ years for the 37 GHz emission relative to the broad lines. From $\overline{\tau}^-_{\rm ob} = -2.86$ years, $R_{\rm BLR} = 2.70$ ly, $v_{\rm d} = 0.9$–$0.995c$, $\theta = 12°$–$21°$ and equation (7), we obtain $R_{\rm radio} = 0.40$–2.62 pc (Case B). These estimated $R_{\rm radio}$ contain the typical size of $R_{\rm BLR} = 0.83$ pc, i.e. the radio emitting regions in Case B are around the BLR. Thus $R_\gamma \lesssim 0.40$–2.62 pc for Case B and these inner emitting regions mostly satisfy $R_\gamma \lesssim R_{\rm BLR}$. For Case D, the special Case B, $R_\gamma \lesssim R_{\rm radio} = 0.77$–$0.81$ pc and $R_\gamma \lesssim R_{\rm BLR}$. The measured positive lags have an average of $\overline{\tau}^+_{\rm cent} = 3.20$ years for the 37 GHz emission relative to the broad lines. From $\overline{\tau}^+_{\rm ob} = 3.20$ years, $R_{\rm BLR} = 2.70$ ly, $v_{\rm d} = 0.9$–$0.995c$, $\theta = 12°$–$21°$ and equation (7), we obtain $R_{\rm radio} = 9.43$–62.31 pc $\gg R_{\rm BLR}$ (Case C). Considering the zero-lag point and the constraint of $R_\gamma \lesssim R_{\rm radio}$, we have 4.67–$30.81 < R_\gamma \lesssim 9.43$–$62.31$ pc for Case C. These outer emitting regions satisfy $R_\gamma \gg R_{\rm BLR}$. The dependence of R_γ and $R_{\rm radio}$ on $v_{\rm d}$ and θ and the allowed intervals of R_γ are presented in Fig. 5. R_γ and $R_{\rm radio}$ increase as $v_{\rm d}$ increases, but decrease as θ increases (see Fig. 5). The uncertainties of $v_{\rm d}$ and θ result in the larger intervals of R_γ and $R_{\rm radio}$. The positions of emitting regions in Cases B and D are consistent with those at sub-pc–pc scales suggested by Blandford & Levinson (1995), Ghisellini & Madau (1996), Kovalev et al. (2009) and Sikora et al. (2009), and also with the dissipative positions at sub-pc-scale proposed by others (Ghisellini & Tavecchio 2009; Ghisellini, Tavecchio & Ghirlanda 2009; Sikora et al. 2009; Ghisellini et al. 2010). The positions of emitting regions in Case C are comparable to those at distances of tens of pc advanced in the recent researches (e.g. Sikora, Moderski & Madejski 2008; Marscher et al. 2010). The relative positions of the BLR and these emitting regions are also consistent with those previous findings. From $\overline{\tau}^-_{\rm ob} = -2.86$ years, $v_{\rm d} = 0.9$–$0.995c$, $\theta = 12°$–$21°$ and equation (10), we obtain $R_{\rm BLR} = 0.77$–0.90 pc, which contain the typical size of $R_{\rm BLR} = 0.83$ pc. These agreements confirm the reliability of the method and assumptions. These inner emitting regions are likely the major contributor of the γ-rays below 10 GeV, and those outer ones are likely the major contributor of the γ-rays above 10 GeV. The method is also applicable to BL Lacs, in which broad lines are detectable, but ionizing continuum is undetectable. The BLR sizes of BL Lacs may be constrained by equation (10).

ACKNOWLEDGMENTS

We are grateful to the anonymous referee for constructive comments and suggestions leading to significant improvement of this paper. H.T.L. thanks the West PhD project of the Training Programme for the Talents of West Light Foundation of the CAS, and National Natural Science Foundation of China (NSFC; Grant 10903025) for financial support. J.M.B. thanks support of NSFC (Grant 10973034). J.M.W. is supported by NSFC (Grant 10733010). J.M.B. and J.M.W. thanks support of the 973 Program (Grant 2009CB824800).

REFERENCES

Abdo A. A. et al., 2009, ApJ, 700, 597
Abdo A. A. et al., 2010a, ApJ, 715, 429
Abdo A. A. et al., 2010b, ApJ, 722, 520
Abdo A. A. et al., 2010c, ApJ, 710, 1271
Abdo A. A. et al., 2010d, Nat, 463, 919
Alexander T., 1997, in Astronomical Time Series, eds, Maoz D., Sternberg A., Leibowitz E. M. (Dordrecht: Kluwer), p. 163
Arshakian T. G., León-Tavares J., Lobanov A. P., Chavushyan V. H., Shapovalova A. I., Burenkov A. N., Zensus J. A., 2010, MNRAS, 401, 1231
Bai J. M., Lee M. G., 2001, ApJ, 558, L19
Bai J. M., Lee M. G., 2003, ApJ, 585, L113
Bai J. M., Liu H. T., Ma, L., 2009, ApJ, 699, 2002
Blandford R. D., Levinson A., 1995, ApJ, 441, 79
Blandford R. D., McKee C. F., 1982, ApJ, 255, 419
Blandford R. D., Payne D. G., 1982, MNRAS, 199, 883
Blandford R. D., Rees M. J., 1978, in Pittsburgh Conf. on BL Lac Objects, ed. Wolfe A. M. (Pittsburgh: Univ. Pittsburgh Press), p. 328
Blandford R. D., Znajek R., 1977, MNRAS, 179, 433
Bloom S. D., 2008, AJ, 136, 1533
Böttcher M., 1999, in AIP Conf. Proc. 515, GeV-TeV Gamma Ray Astrophysics Workshop, ed. Dingus B. L., Salamon M. H., Kieda D. B. (New York: AIP), p. 31
Böttcher M., 2008, in AIP Conf.Proc. 1085, High Energy Gamma-Ray Astronomy, p. 427
Cao X. W., Jiang D. R., 1999, MNRAS, 307, 802
Cao X. W., Jiang D. R., 2001, MNRAS, 320, 347

Celotti A., Padovani P., Ghisellini G., 1997, MNRAS, 286, 415
Chaterjee R. et al., 2009, ApJ, 704, 1689
Courvoisier T. J. L. et al., 1990, A&A, 234, 73
Courvoisier T. J. L., 1998, A&ARv, 9, 1
Davis R. J., Unwin S. C., Muxlow T. W. B., 1991, Nat, 354, 374
Dermer C. D., Schlickeiser R., 1994, ApJS, 90, 945
Edelson R. A., Krolik J. H., 1988, ApJ, 333, 646
Edelson R. A. et al., 1996, ApJ, 470, 364
Elvis M., Risaliti G., Zamorani G., 2002, ApJ, 565, L75
Falcke H., Malkan M. A., Biermann P. L., 1995, A&A, 298, 375
Ferland G. J., Korista K. T., Verner D. A., Ferguson J. W., Kingdon J. B., Verner E. M., 1998, PASP, 110, 761
Fossati G., Maraschi L., Celotti A., Comastri A., Ghisellini G., 1998, MNRAS, 299, 433
Gaskell C. M., Peterson B. M., 1987, ApJS, 65, 1
Georganopoulos M., Kirk J. G., Mastichiadis A., 2001, in ASP Conf. Series 227, Blazar Demographics and Physics, Ed. Padovani P., Urry C. M. (San Francisco: Astronomical Society of the Pacific), p. 116
Georganopoulos M., Perlman E. S., Kazanas D., McEnery J., 2006, ApJ, 653, L5
Ghisellini G., Madau P., 1996, MNRAS, 280, 67
Ghisellini G., Celotti A., Fossati G., Maraschi L., Comastri A., 1998, MNRAS, 301, 451
Ghisellini G., Maraschi L., Tavecchio F., 2009, MNRAS, 396, L105
Ghisellini G., Tavecchio F., 2009, MNRAS, 397, 985
Ghisellini G., Tavecchio F., Foschini L., Ghirlanda G., Maraschi L., Celotti A., 2010, MNRAS, 402, 497
Ghisellini G., Tavecchio F., Ghirlanda G., 2009, MNRAS, 399, 2041
Giveon U. et al., 1999, MNRAS, 306, 637
Gu M. F., Cao X. W., Jiang, D. R., 2009, MNRAS, 396, 984
Jorstad S. G. et al., 2001, ApJ, 556, 738
Jorstad S. G. et al., 2007, AJ, 134, 799
Kaspi S., Brandt W. N., Maoz D., Netzer H., Schneider D. P., Shemmer O. A., 2007, ApJ, 659, 997
Kaspi S., Maoz D., Netzer H., Peterson B. M., Vestergaard M., Jannuzi B. T., 2005, ApJ, 629, 61
Kaspi S., Netzer H., 1999, ApJ, 524, 71
Kaspi S., Smith P. S., Netzer H., Maoz D., Jannuzi B. T., Giveon U., 2000, ApJ, 533, 631
Koide S., Shibata K., Kudoh T., Meier D. L., 2002, Sci, 295, 1688
Koide S., 2004, ApJ, 606, L45
Komissarov S. S., 2002, MNRAS, 336, 759
Komissarov S. S., 2004, MNRAS, 350, 1431
Kovalev Y. Y. et al., 2009, ApJ, 696, L17
Kudoh T., Matsumoto R., Shibata K., 1998, ApJ, 508, 186
Kudoh T., Shibata K., 1999, ApJ, 514, 493
Lichti G. G. et al., 1995, A&A, 298, 711
Lind K. R., Blandford R. D., 1985, ApJ, 295, 358
Lindfors E. J., Valtaoja E., Türler M., 2005, A&A, 440, 845
Liu H. T., Bai J. M., 2006, ApJ, 653, 1089
Liu H. T., Bai J. M., Ma L., 2008, ApJ, 688, 148
Liu H. T., Bai J. M., Zhao X. H., Ma L., 2008, ApJ, 677, 884
Marscher A. P., Jorstad, S. G., Gómez, J. L., Aller, M. F., Teräsranta, H., Lister, M. L., Stirling, A. M., 2002, Nat, 417, 625
Marscher A. P. et al., 2010, ApJ, 710, L126
McKinney J. C., 2006, MNRAS, 367, 1797
Meier D. L., Koide S., Uchida Y., 2001, Sci, 291, 84
Paltani S., Courvoisier T. J. L., Walter R., 1998, A&A, 340, 47
Paltani S., Türler M., 2005, A&A, 435, 811
Penrose R., 1969, Nuovo Cimento Rivista, 1, 252
Peterson B. M. et al., 2000, ApJ, 542, 161
Peterson B. M. et al., 2004, ApJ, 613, 682
Peterson B. M. et al., 2005, ApJ, 632, 799
Pyatunina T. B., Kudryavtseva N. A., Gabuzda D. C., Jorstad S. G., Aller M. F., Aller H. D., Teräsranta H., 2006, MNRAS, 373, 1470
Pyatunina T. B., Kudryavtseva N. A., Gabuzda D. C., Jorstad S. G., Aller M. F., Aller H. D., Teräsranta H., 2007, MNRAS, 381, 797
Rawlings S., Saunders R., 1991, Nat, 349, 138
Robson E. I. et al., 1993, MNRAS, 262, 249
Roy M., Papadakis I. E., Ramos-Colon E., Sambruna R., Tsinganos K., Papamastorakis J., Kafatos M., 2000, ApJ, 545, 758
Semenov V., Dyadechin S., Punsly B., 2004, Sci, 305, 978
Serjeant S. et al., 1998, MNRAS, 294, 494
Schmidt M., 1963, Nat, 197, 1040
Shields G. A., 1978, Nat, 272, 706
Sikora M., Moderski R., Madejski G. M., 2008, ApJ, 675, 71
Sikora M., Stawarz L., Moderski R., Nalewajko K., Madejski G. M., 2009, ApJ, 704, 38
Sitarek J., Bednarek W., 2008, MNRAS, 391, 624
Sokolov A., Marscher A. P., 2005, ApJ, 629, 52
Soldi S. et al., 2008, A&A, 486, 411
Tavares J. L., Lobanov A. P., Chavushyan V. H., Arshakian T. G., Doroshenko V. T., Sergeev S. G., Efimov Y. S., Nazarov S. V., 2010, ApJ, 715, 355
Tavecchio F., Ghisellini G., Bonnoli G., Ghirlanda G., 2010, MNRAS, 405, L94
Tavecchio F., Mazin D., 2009, MNRAS, 392, L40
Thompson D. J., 2008, Rep. Prog. Phys., 71, 6901
Torres D. F., Romero G. E., Barcons X., Lu Y. J., 2003, ApJ, 596, L31
Türler M. et al., 1999, A&AS, 134, 89
Türler M., Courvoisier T. J. L., Paltani S., 2000, A&A, 361, 850
Ulrich M. H., Maraschi L., Urry C. M., 1997, ARA&A, 35, 445
Unwin S. C. et al., 1985, ApJ, 280, 109
Vestergaard M., Peterson B. M., 2006, ApJ, 641, 689
von Montigny C. et al., 1997, ApJ, 483, 161
Wagner R. M., 2008, MNRAS, 385, 119
Wandel A., Peterson B. M., Malkan M. A., 1999, ApJ, 526, 579
Wang J. M., 2000, ApJ, 538, 181
Wang J. M., Ho L. C., 2003, A&A, 409, 887
Yaqoob T., Serlemitsos P., 2000, ApJ, 544, L95
Zhang J., Bai J. M., Chen L., Liang E. W., 2010, ApJ, 710, 1017
Zhang J., Bai J. M., Chen L., Yang X., 2009, ApJ, 701, 423